View metadata, citation and similar papers at core.ac.uk

brought to you by CORE

provided by Missouri University of Science and Technology (Missouri S&T): Scholars' Mine

Missouri University of Science and Technology

Scholars' Mine

Electrical and Computer Engineering Faculty Research & Creative Works

Electrical and Computer Engineering

01 Sep 1993

# Transition Mechanisms of Two Interacting DX Centers in N-Type AlGaAs using Reverse-Bias Deep Level Transient Spectroscopy and Temperature-Dependent Pulse-Width Reverse-Bias Deep Level Transient Spectroscopy Methods

C. W. Wang

Cheng-Hsiao Wu
*Missouri University of Science and Technology*, chw@mst.edu

Follow this and additional works at: https://scholarsmine.mst.edu/ele_comeng_facwork

Part of the Electrical and Computer Engineering Commons

## Recommended Citation

C. W. Wang and C. Wu, "Transition Mechanisms of Two Interacting DX Centers in N-Type AlGaAs using Reverse-Bias Deep Level Transient Spectroscopy and Temperature-Dependent Pulse-Width Reverse-Bias Deep Level Transient Spectroscopy Methods," *Journal of Applied Physics*, vol. 74, no. 6, pp. 3921-3926, American Institute of Physics (AIP), Sep 1993.
The definitive version is available at https://doi.org/10.1063/1.354491

This Article - Journal is brought to you for free and open access by Scholars' Mine. It has been accepted for inclusion in Electrical and Computer Engineering Faculty Research & Creative Works by an authorized administrator of Scholars' Mine. This work is protected by U. S. Copyright Law. Unauthorized use including reproduction for redistribution requires the permission of the copyright holder. For more information, please contact scholarsmine@mst.edu.

# Transition mechanisms of two interacting *DX* centers in *N*-type AlGaAs using reverse-bias deep level transient spectroscopy and temperature-dependent pulse-width reverse-bias deep level transient spectroscopy methods

C. W. Wang and C. H. Wu
*Department of Electrical Engineering, University of Missouri-Rolla, Rolla, Missouri 65401*

(Received 27 October 1992; accepted for publication 26 May 1993)

The reverse-bias pulsed deep level transient spectroscopy (RDLTS) and a new temperature-dependent pulse-width RDLTS (TDP RDLTS) technique are reported to study the electric-field effect on carrier emission rates and the direct interaction between double *DX* centers recently detected in the Se:$Al_{0.6}Ga_{0.4}As$ *N* confinement layer of the AlGaAs/GaAs single-quantum-well laser diodes. Traditional RDLTS measurements, with constant pulse width $t_p$, prove that the two *DX* centers, $Et_1$ and $Et_2$, have strong direct emission interaction. Furthermore, the new TDP-RDLTS technique enables one to evaluate this direct transition time constant. Possible mechanisms for this interstate transition at different temperature ranges are provided and the new broadening effect due to this interstate transition is also reported here for the first time. Field-enhanced emission rates are calculated.

## I. INTRODUCTION

Study of the deep level defects in semiconductors is extremely important, since the presence of the defects significantly affects the device performance. Today, the device fabrication technology has advanced to submicrometer ranges for fabricating higher-speed and higher-frequency devices and circuits. Thus, the average electric field used in operating these devices is high, and defects subjected to high electric fields can degrade device performance. In a traditional deep level transient spectroscopy (DLTS) measurement,[1] the emission signal comes from the entire depletion region, where the electric field varies with position. Therefore, even if the density of the trap is uniformly distributed, the capacitance transient signal, which comes from the total amount of emission charges, is contributed from nonuniformly distributed emission rates from the zero-field region at the depletion layer edge to the region with maximum junction field. This produces a nonexponential transient signal, and the measured activation energies are subjected to error.[2,3] Although several methods were proposed to reduce the error due to this field effect, none of the methods were convenient to use, and none provided accurate results.[4–6]

Reverse-bias deep level transient spectroscopy (RDLTS) has been shown to be both a convenient and an accurate method for determining the electric-field dependence of emission rate from a deep level trap.[7,8] The principle of this technique is to use a reverse-bias pulse to superimpose on a reverse dc bias, in contrast with the use of a forward-bias pulse in a conventional DLTS setup. The transient signal observed is from the capturing of carriers by the deep level states located in an extremely narrow region where the electric field can be accurately controlled.[7] In Refs. 7 and 8, the authors effectively calculated the enhanced emission rate due to this high-electric-field effect for a single deep trap in In-doped Si samples. Recently, the direct interaction between two *DX* centers has been observed for the first time in *N*-type Se:$Al_{0.6}Ga_{0.4}As$ material.[9] In Ref. 9, we use the RDLTS technique to show that the total electron emission during the reverse-bias pulse is not equal to the total electron capture after the pulse is turned off. This is in contrast with the observation in a single-trap case, where the equality has been established by Li and Wang.[7,8] In their work, a saturated RDLTS peak is observed for a single trap when the applied reverse-biased pulse width $t_p$ is increased. In the case of two *DX* centers, we observed, however, a nonsaturated RDLTS peak as $t_p$ was increased. This is because an electron in the deeper trap level can make direct transition to the shallower one during the emission process, so that the net emission rate is increased in addition to the high-electric-field effect, as observed in Refs. 7 and 8. The mechanism of this direct electronic transition between the two *DX* centers and their enhanced emission rates has not been investigated.

The purpose of this work is to provide a new insight into the interaction mechanisms of the double *DX* centers under different applied pulse widths by using the traditional RDLTS and the improved temperature-dependent pulsewidth (TDP)-RDLTS techniques. In Sec. II, the experimental arrangement and RDLTS theoretical principles are described. We also show that our TDP-RDLTS technique is an effective method to evaluate the transition time constant. Establishing the transition mechanisms for the double *DX* centers is presented in Sec. III, and conclusions are addressed in Sec. IV.

## II. EXPERIMENTAL DETAILS AND THEORETICAL BACKGROUND

In this work we use the RDLTS technique to identify the enhanced emission rate under high electric field, and the emission rate due to an interaction between two *DX* centers. The RDLTS signals are from Se:$Al_{0.6}Ga_{0.4}As$ *N*

 0021-8979/93/74(6)/3921/6/$6.00 © 1993 American Institute of Physics 

confinement layer of the AlGaAs/GaAs graded-index-separate-confinement-heterostructure–single-quantum-well (GRINSCH-SQW) laser diodes grown by a metal-organic chemical-vapor deposition (MOCVD) method. The detailed device structure and chemical composition are described elsewhere.[9] In contrast to the conventional DLTS, a relatively low bias $V_r$ is used for establishing a low electric field in this technique. It has been shown that RDLTS measurements possess the advantages of the high detection sensitivity and spatial resolution.[8] By considering both the emission mechanism during the application of the emission pulse and the capture dynamics during the capacitance transient observation, the capacitance transient signal can be expressed as[7,10]

$$\frac{\Delta C(t)}{C}=\int_0^1 (1-z)\frac{N_t(z)}{N_D(z)}\left[1-\exp\left(-\frac{t_p}{\tau_e(z,\epsilon)}\right)\right]\times\exp\left(-\frac{t}{\tau_c(z)}\right)dz \qquad (1)$$

and

$$z=1-x/w,$$

where $x$ is the position of defects inside the depletion region, and $w$ is the depletion width. Both defect and shallow dopant concentrations $N_t$ and $N_D$ are functions of distance. It is noted that $z$ is a dimensionless coordinate running from 0 to 1. The two factors, $\tau_e(z,\epsilon)$ and $t_p$, inside the integral are the emission time constant and the emission pulse width, respectively. These two factors control the transient signal amplitude. The transient observation time $t$ and the spatial dependent capture rate $\tau_c(z)$ also control the measured transient signal amplitude. In such a measurement, electrons are captured within a narrow region of the depletion region, centered at $x_0$, the point of intersection of the Fermi level and the defect level at the reverse dc bias $V_r$. A detailed description of the mechanisms of emission and capture is given in Ref. 7. It is noted that Eq. (1) is valid only when $\Delta C \ll C$, and this condition is satisfied in our measurements. Since the transient capacitance signal comes mainly from the capture of electrons by the defects centered in a narrow region of $x=x_0$, the

$$N_t(z)\{1-\exp[-t_p/\tau_e(z,\epsilon)]\}$$

factor can be moved outside of the integral, and Eq. (1) is written as

$$\frac{\Delta C(t)}{C}=N_t\left[1-\exp\left(-\frac{t_p}{\tau_e(\epsilon)}\right)\right]_{x=x_0}\int_0^1 dz\times\exp\left(-\frac{t}{\tau_c(z)}\right)\frac{1-z}{N_D(z)}. \qquad (2)$$

The relation of $\Delta C\propto N_t\{1-\exp[-t_p/\tau_e(\epsilon)]\}$ is valid for our measurements where the RDLTS signals are from the $n$-type region of the laser diode only. We also note that the quantum-well region is a very thin undoped layer. If we consider the quantum-well region as a continuously distributed trap site, the emission from and capture into the quantum well is negligible. This is due to the fact, at the reverse-bias voltages used in the measurement, that the depletion edge is always well outside of the quantum-well region.

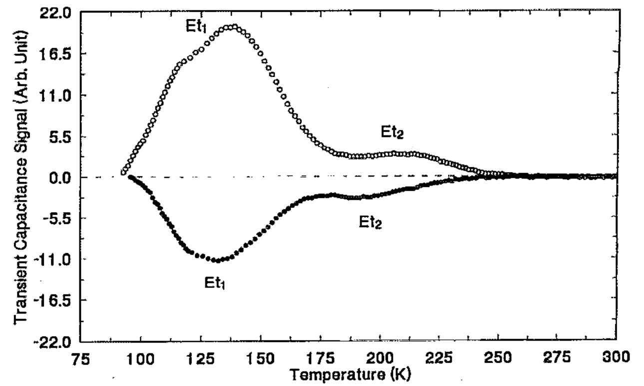


FIG. 1. Typical DLTS and RDLTS signals of GRINSCH SQW with pulse width $t_p$=100 ms; $t_2/t_1$=60, $t_2$=3 ms for both curves. The open-circle curve is for DLTS at $V_r$=−3 V and $V_p$=0.5 V; the solid-circle curve is for RDLTS at $V_r$=−0.5 V and $V_p$=−3 V.

## III. RESULTS AND DISCUSSION

In our GRINSCH-SQW laser diodes two deep electron traps inside the $n$-type Se:$Al_{0.6}Ga_{0.4}As$ confinement region have been detected by DLTS measurement as shown in Fig. 1. We note that the added complexities of the quantum well do not increase the difficulty in detecting the defects and impurities in the $n$-type region. The corresponding activation energies are $Et_1 \cong E_c-0.28$ eV and $Et_2\cong E_c-0.43$ eV, respectively. The typical RDLTS spectra are also depicted in Fig. 1. In our earlier work,[9] we demonstrated that these two deep traps are all $DX$ centers with strong emission interaction between each other by the evidence of conventional RDLTS results as shown in Fig. 2. In Fig. 2, we observe that the $Et_1$ peak increases its height with increasing pulse width to a maximum, then

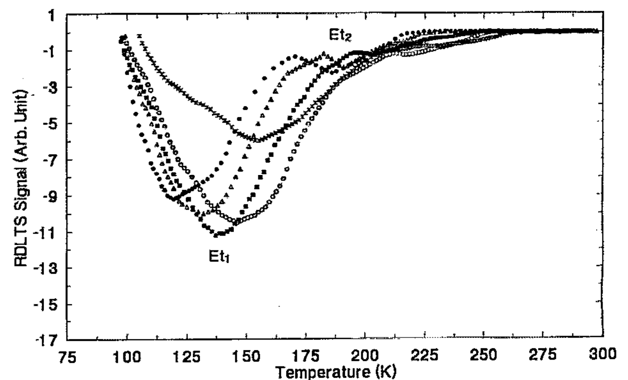


FIG. 2. RDLTS signals of GRINSCH SQW under different pulse width $t_p$ and with the same pulse voltage $V_p$=−3 V, $V_r$=−0.5 V ($\tau_d$=8.03 ms). Note that once $Et_1$ reaches the saturation peak at $t_p=\tau_d$, the peak starts to decrease with increasing $t_p$. ●: $t_p=100\tau_d$; △;$t_p=10\tau_d$; ■: $t_p=1\tau_d$; ○:$t_p=0.1\tau_d$; and *:$t_p=0.01\tau_d$.

decreases. The $Et_2$ peak, from a vague situation, becomes gradually clear with increasing pulse, $t_p$, especially when $t_p \gg \tau_d$. If $Et_1$ and $Et_2$ are spatially independent traps, then from Eq. (2) as the emission pulse width $t_p$, goes longer, the emission term $\{1 - \exp[-t_p/\tau_e(\epsilon)]\}|_{x=x_0}$ becomes larger until it reaches the maximum value. In this situation, constant pulse-width RDLTS measurements should indicate that the $Et_1$ or $Et_2$ peak increases its amplitude with increasing pulse width until it reaches a saturation height. This is the case for one type of *DX* center in In-doped Si samples that has been reported by Li and Wang in Ref. 8. However, our RDLTS results clearly show that the $Et_1$ trap has an obvious nonsaturated, or decreasing, peak, when the pulse width $t_p$ becomes longer. The reduced strengths of the $Et_1$ peak, when $t_p \gg 8.03$ ms, stronger reveal that the depopulation of the $Et_1$ trap during the emission process is greater than the repopulation during the capture process. The only possible reason for this result is that when $t_p$ becomes longer, the $Et_2$ trap has the possibility to direction emit electrons into the $Et_1$ trap during the reverse-biased pulse-width duration (i.e., the emission process). As a result, less electrons from the conduction band are needed to return to the $Et_1$ trap in the capture process when the reverse-biased pulse is turned off. Hence, the $Et_1$ peak cannot reach a saturated height when $t_p \gg 8.03$ ms. We therefore conclude that the $Et_1$ and $Et_2$ traps have direct interstate transition and, consequently, they must all be *DX* centers. The occurrence of more than one *DX*-type deep level trap in $Al_xGa_{1-x}As$ has also been proposed by the earlier investigators.[11–14] One possible explanation for the nature of these two interacting *DX* centers is that both centers are spatially close to each other so that they form atomiclike states associated with the trap levels. Therefore, a direct interstate transition is possible without going through the conduction band.

To determine the transition time constant, and to further establish the possible transition mechanisms for these two *DX* centers, we developed a novel technique to improve the traditional RDLTS measurement. In the traditional RDLTS technique, the pulse width $t_p$ is set to maintain a constant value during the entire temperature scan. In our previous work,[9] the emission time constants of the $Et_1$ and $Et_2$ traps have been calculated as functions of temperature from DLTS measurement under a condition where a reverse bias $V_r = -3$ V and a pulse voltage $V_p = -0.5$ V. The results are

$$\tau_{e_1} \cong 10^{**}(-0.082\,27T + 12.221\,77)\ \text{s}$$

and

$$\tau_{e_2} \cong 10^{**}(-0.055\,13T + 11.798\,83)\ \text{s},$$

respectively, and $T$ is temperature in K. Hence, it is very important to set the emission pulse width $t_p$ as a function of temperature in order to obtain more information. We have successfully applied the TDP-DLTS method (by setting the pulse width $t_p$ to follow the temperature-dependent capture time constant curve with a proper proportional constant) to block the direct interaction between the $Et_1$ and $Et_2$ traps. The activation energy of the pure $Et_1$ trap, without an interaction effect from the $Et_2$ trap, was obtained as $Et_1(\text{pure}) \cong 0.26$ eV which is a little shallower than 0.28 eV (measured by traditional constant pulse-width DLTS method). The details of the TDP-DLTS technique are given in Ref. 9.

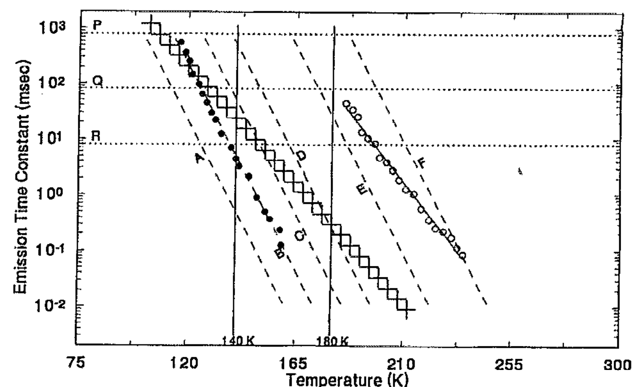


FIG. 3. Emission time constant of $Et_1$ and $Et_2$ traps, as well as 21 different pulse-width curves. Three constant pulse widths are marked as P (803 ms), $Q$ (80.3 ms), and R (8.03 ms). Six temperature-dependent pulses are: P-A, P-B, P-C, P-D, P-E, and P-F, respectively, where the P-A pulse is first set at a constant width (803 ms) at a lower-temperature range and then followed by a temperature-dependent pulse width along the curve A. Similarly, six temperature-dependent pulses are Q-A through Q-F. The last six pulses are R-A through R-F. The symbol marked by + is the estimated transition time constants from $Et_2$ to $Et_1$. The curve fittings are: ●:$\log(\tau_{e1}) = -0.082\,27 + 12.221\,77$; and ○:$\log(\tau_{e2}) = -0.055\,13T + 11.798\,83$. The dotted lines of A, B, C, D, E, and F are for $0.1\tau_{e_1}, 1\tau_{e_1}, 10\tau_{e_1}, 10^2\tau_{e_1}, 10^4\tau_{e_1}$, and $10^6\tau_{e_1}$, respectively. The region between two vertical lines marked by 140 and 180 K is the medium temperature for Fig. 8.

In this article, we show that by using our newly developed TDP-RDLTS technique, it is possible to determine the interstate transition time constant between the double *DX* centers, and also to establish the transition mechanisms for them. Figure 3 shows the emission time constant as a function of temperature and the applied pulse-width curves with their upper pulse width limits. Data were taken (with fixed pulse width and with the pulse width set to follow the emission time constant of the $Et_1$ trap) with six different multipliers: $m = 0.1$, 1, 10, $10^2$, $10^4$, and $10^6$ (marked A–F, respectively in Fig. 3). In the measurements, the maximum pulse widths were limited to 803, 80.3, and 8.03 ms (marked P, Q, and R, respectively, in Fig. 3) by the pulse generator. The RDLTS results, under the above different pulse-width curves, are shown in Figs. 4–6, from which we observe a consistent result. If the pulse-width follows a smaller multiplier (i.e., $m = 0.1$ or 1), $Et_1$ shows a partially emitted peak. At $m = 10$, the $Et_1$ peak reaches a saturated height and then becomes broader with increasing multipliers. We note that we observe the $Et_2$ peak only when $m = 10^6$ or a constant pulse width is applied. This is because when a pulse width corresponding to $m = 10^6$ or a large enough constant pulse width is applied, the emission time constant of the $Et_2$ trap is always shorter than the time of applied pulses, except at the low-temperature range (as indicated by curves P, Q, R, R-F, Q-F, and P-F in Fig.

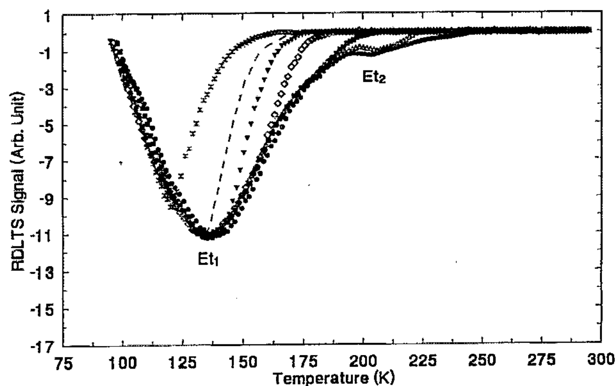


FIG. 4. RDLTS signals measured with fixed pulse width $t_p$ and with the pulse width set to follow the emission time constant of $Et_1$ trap with six different multipliers: $m=0.1,1,10,10^2,10^4$, and $10^6$. (Those are R-A through R-F curves in Fig. 3, respectively). The upper pulse-width limits are 8.03 ms. Pulse voltage $V_p=-3$ V, $V_r=-0.5$ V ($t_2/t_1=500$, $t_2=50$ ms). ●: (curve R); △: (curve R-F); ■: (curve R-E); ◇: (curve R-D); ▼: (curve R-C); – –: (curve R-B); and *: (curve R-A) from Fig. 3.

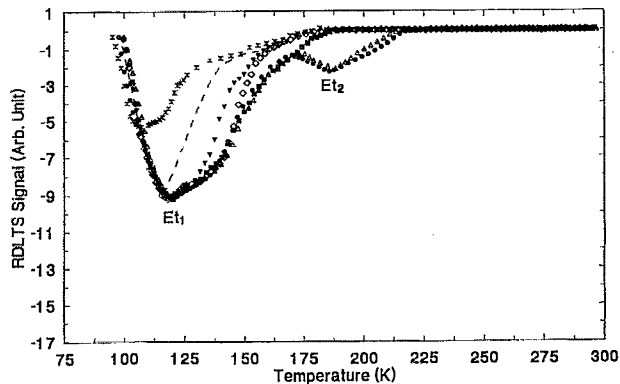


FIG. 6. RDLTS signals measured with fixed pulse width $t_p$ and with the pulse width set to follow the emission time constant of $Et_1$ trap with six different multipliers: $m=0.1$, 1, 10, $10^2$, $10^4$, and $10^6$ (P-A through P-F curves in Fig. 3, respectively). The upper pulse-width limits are 803 ms. Pulse voltage $V_p=-3$ V, $V_r=-0.5$ V ($t_2/t_1=500$, $t_2=50$ ms). ●: curve P; △: curve P-F; ■: curve P-E; ◇: curve P-D; ▼: curve P-C; – –: curve P-B; and * curve P-A from Fig. 3.

3). In Fig. 7, we provide unambiguous results to indicate the existence of direct interaction between the $Et_1$ and $Et_2$ traps. From this figure we clearly observe three trends: (i) At $T<140$ K, the $Et_1$ peak decreases its height with increasing pulse width (curves a, c, and e in Fig. 7); (ii) at $140\ \mathrm{K}<T<180$ K, the $Et_1$ peak is broader when compared to curves with constant pulse widths (curves a, c, and e) than to those with pulse-width settings that follow the $10\tau_{e_1}$curve (curves b, d, and f); and (iii) at $T>180$ K, the $Et_2$ peak cannot be observed when the pulse widths follow the $10\tau_{e_1}$ curve (curves b, d, and f). From Fig. 7, we conclude that the direct-transition time constant between the two *DX* centers is in the range between $\tau_{e_1}$ and $\tau_{e_2}$, as marked by the symbol + shown in Fig. 3. This estimation is made from data provided in Fig. 7.

To explain the results of Fig. 7, we propose mechanisms of direct transition between the double *DX* centers. The mechanisms of direct interstate transition, divided into three different temperature ranges (for $T<140$ K, $140\ \mathrm{K}<T<180$ K, $T>180$ K) are sketched in Fig. 8. The capture cross sections of $Et_1$ and $Et_2$ are temperature dependent as discussed in Ref. 9. The DLTS peak for $Et_2$ is small and it is difficult to locate the peak location, especially at a partial-filling pulse; however, the estimated activation barrier of the capture cross section of $Et_2$ is very sensitive to temperature change. This is in contrast with the capture cross section of $Et_1$, which is shown in Ref. 9, in the range of our experiment. Here, despite the complex nature of the $Et_2$ capture cross section, we are able to propose a consistent interstate transition mechanism to explain the observation of Fig. 7. At the low-temperature

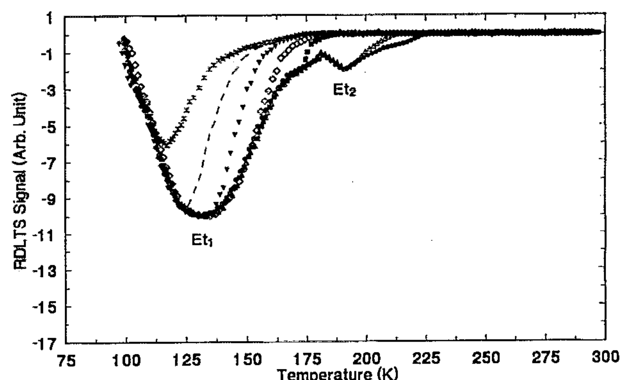


FIG. 5. RDLTS signals measured with fixed pulse width $t_p$ and with the pulse width set to follow the emission time constant of $Et_1$ trap with six different multipliers: $m=0.1$, 1, 10, $10^2$, $10^4$, and $10^6$ Q-A through Q-F curves in Fig. 3, respectively. The upper pulse-width limits are 80.3 ms. Pulse voltage $V_p=-3$ V, $V_r=-0.5$ V ($t_2/t_1=500$, $t_2=50$ ms). ●: curve Q; △: curve Q-F; ■: curve Q-E; ◇: curve Q-D); ▼: curve Q-C; – –: curve Q-B; and *: curve Q-A from Fig. 3.

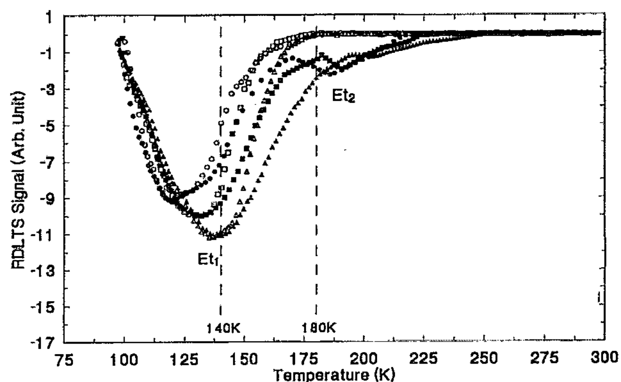


FIG. 7. RDLTS signals measured with fixed pulse width $t_p$ (P,Q, and R curves in Fig. 3) and with the pulse width set to follow the emission time constant of $Et_1$ trap with six multipliers $m=10$ (curves P-C, Q-C, and R-C refer to Fig. 3). Pulse voltage $V_p=-3$ V, $V_r=-0.5$ V ($t_2/t_1=500$, $t_2=50$ ms). ●: curve P; ○: curve P-C; ■: curve Q; □: curve Q-C; ▲: curve R; and △: curve R-C from Fig. 3. The region between two vertical dotted lines marked by 140 and 180 K is the medium temperature range for Fig. 8.

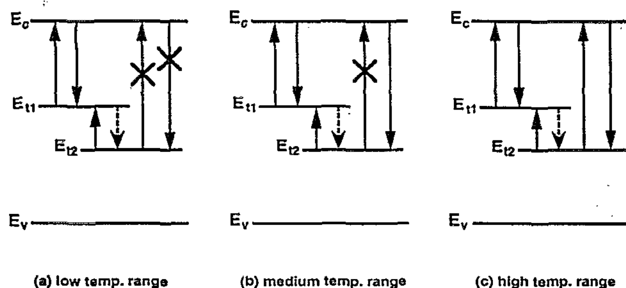


FIG. 8. The interstate state transition mechanisms in three different temperature ranges: (a) low-temperature range (temperature $< 140$ K); (b) medium temperature range (temperature $> 180$ K). The symbol marked by × means such a transition does not occur within the measuring time and the process with dashed arrow line means a much smaller probability of occurrence as compared to that of the opposite direction.

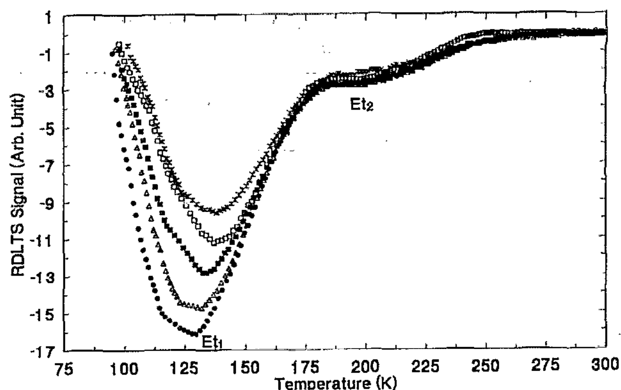


FIG. 9. RDLTS signals of the laser diodes under different pulse voltage $V_p$ and with the same pulse duration $t_p = \tau_d = 8.03$ ms ($t_2/t_1 = 500$, $t_2 = 50$ ms). The strong enhancement of the emission rate is shown by the increase of the RDLTS signals as reverse voltage $V_p$ increases. ●: $V_p = -7.5$ V and $V_r = -0.5$ V; △: $V_p = -6.0$ V and $V_r = -0.5$ V; ■: $V_p = -4.5$ V and $V_r = -0.5$ V; □: $V_p = -3.0$ V and $V_r = -0.5$ V; and *: $V_p = -1.0$ V and $V_r = -0.5$ V, respectively.

range of the measurement, there is a net emission of the $Et_2$ trap into the $Et_1$ trap, and a very low possibility of emitting electrons directly into the conduction band or the probability of capturing electrons from the conduction band because the emission time or the capture time is much longer than the measuring time. In the RDLTS experiment, the electron population of the trap is first decreased during the emission pulse duration. Through a subsequent capture process, right after the pulse is turned off, the RDLTS measures the degree of trap depopulation by restoring the trap occupancy back to its original amount. At $T < 140$ K, if the pulse width is increased from 8.03 ms to 803 ms, we observe a decrease of the $Et_1$ peak. Because electrons from the $Et_2$ trap can make a direct transition to $Et_1$, there is a reduced electron-capture process of the $Et_1$ trap; hence, the decrease of RDLTS signals is observed. This indicates a higher possibility for the $Et_2$ trap to emit electrons directly to the $Et_1$ trap. As a result, the transient capacitance $\Delta C$ decreases and a smaller $Et_1$ peak is obtained when $t_p$ is greater than 8.03 ms (curves a, c, and e in Fig. 7 at $T < 140$ K). We note that if there is no such direct transition, the $Et_1$ peak should remain saturated, which is not observed in this experiment. In other words, the depopulation of the electron is equal to the repopulation of the electron for the $Et_1$ trap if there is no direct transition between $Et_1$ and $Et_2$. At the medium temperature range, the $Et_2$ trap can emit electrons into the $Et_1$ trap and capture electrons from the conduction band, but with negligible possibility of emitting electrons directly into the conduction band within the measuring time. In this situation, if the pulse width is greater than the estimated transition time constant, the signal of transient capacitance $\Delta C$ will be larger. As a result, a broader $Et_1$ peak can be detected. The broadenings of the $Et_1$ peak, at temperatures between 140 and 180 K, are shown in Fig. 7 when curve a is compared to curve b, curve c to curve d, and curve e to curve f, respectively. Thus, we show, for the first time, a new type of broadening effect due to the direct interstate transition of two *DX* centers, and that this type of broadening is quite different from the "alloy broadening effect" in *DX* centers. The latter is based on different atom arrangements around the defects,[15–17] or the different possible orientations of the defect symmetry axis with the applied electric field.[18] At the high temperature range, the $Et_2$ trap can emit electrons into both the $Et_1$ trap and the conduction band, as well as capturing electrons directly from the conduction band. This is the reason why we can observe the $Et_2$ peak in the RDLTS measurements as long as the pulse width $t_p$ is greater than the emission time constant of the $Et_2$ trap.

It is well known that the electric field can reduce the potential well of the defect and alter the emission-capture process of carriers from deep level defects.[19–24] Most articles are based on the mechanism of the Poole–Frenkel effect, where the electron emission takes place over a Poole–Frenkel-type potential well, which can be lowered by the presence of the electric field.[25] To show that the electric field in the depletion region has a great influence on the emission rate of the deep traps, we apply a different height of emission pulse voltage $V_p$ to the devices, while keeping the pulse width $t_p$ at a fixed value. The results are shown in Fig. 9. We define $\tau_e^0$ as the low-field-emission time constant. It is set to equal the detection time constant given by $(t_2\text{-}t_1)/\ln(t_2/t_1)$. Figure 9 shows that larger amplitudes of the RDLTS capacitance transient signal and lower peak temperatures of the $Et_1$ peak are obtained with the increasing emission pulse voltages. It indicates that the larger emission pulse voltage, the higher electric field, and the smaller emission time constant $\tau_e^*$ are obtained. Furthermore, from Eq. (2), if we set the same reverse dc bias voltage $V_r$ and the same sampling time $t_1$ and $t_2$, $\Delta C(t)/C$ will be proportional to $\{1 - \exp[-t_p/\tau_e(\epsilon)]\}|_{x=x_0}$ under different applied emission pulse voltages. Recall that $x_0$ is the point of intersection of the Fermi level and the defect level at the reverse dc bias $V_r$. Consequently, the electric-field-enhanced emission rate can be measured directly from the transient capacitance amplitudes. The field in the extremely narrow detection region can be calculated from the pulse heights. The spatial variations of $N_D$ and $N_t$, if any, do not affect the measurement accuracy because the signal comes only from a fixed localized region. An easy way to

TABLE I. Selected experimental pulse widths and heights for obtaining the same RDLTS $Et_1$ peak amplitude.

| Pulse width (ms) | Pulse voltage $V_p$ (V) |
|---|---|
| 8.03 | −1 |
| 1.665 | −2 |
| 0.845 | −3 |
| 0.310 | −4.5 |
| 0.185 | −6 |
| 0.120 | −7.5 |

measure the electric-enhanced emission rate is to change the emission pulse height and width simultaneously, while the transient capacitance signal amplitude is kept at a constant.[8] The ratio of the emission pulse widths from the low-field to the high-field cases are then used to calculate the enhanced emission rate. By choosing the proper width for various pulse heights, the same RDLTS amplitude for the $Et_1$ trap can be obtained. This is illustrated in Table I. The enhanced emission rates, at the relative low-field-emission rate (at $V_p=-1$ V), are calculated and shown in Fig. 10. Note that this enhancement is not due to the high-electric-field effect only, as reported in Ref. 8 in the case of a single trap. Our observed increase of the emission rate is a result of both the high electric field and the direct transition between two *DX* centers. Since the minor peak $Et_2$ is always too small, it is not accurate enough to measure the enhanced emission rate for the $Et_2$ trap in our technique.

## IV. CONCLUSIONS

The conventional RDLTS and the newly developed TDP-RDLTS techniques are reported for investigating the direct interstate transition between double *DX* centers, as well as the electric-field effect on carrier emission from these two *DX* centers as detected in GRINSCH-SQW laser diodes. Traditional RDLTS measurement results show that the $Et_1$ and $Et_2$ traps have strong direct interaction between these two trap levels. From the TDP-RDLTS measurement results, we further establish the mechanisms of direct transition between these two traps at various temperature ranges and successfully explain the interaction phenomena, as well as a new type of broadening effect, due to such a interstate transition, reported here for the first time.

The RDLTS results also indicate that the emission rate is increased further at high field, even in the presence of two interacting deep traps, which in turn implies a shorter effective carrier generation lifetime. In very large-scale integrated technology, devices are scaled down, and the enhancement in carrier emission from the defects can cause an immature breakdown and an increase in leakage current under a reverse-bias conduction.

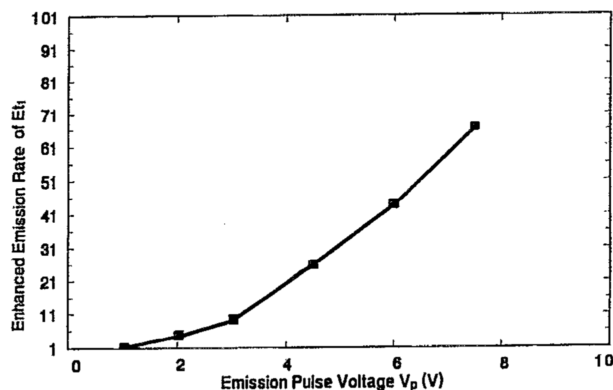


FIG. 10. Enhanced emission rate relative to low-field emission rate for $Et_1$ as a function of reverse emission pulse height at temperature =138 K [$\tau_e^0$ is the emission time constant at low negative field $V_p=1$ V; $\tau_e^*$ is the emission time constant at higher emission pulse voltage $V_p$ and the vertical axis is the ratio $(\tau_e^*/\tau_e^0)^{-1}$].


[1] D. V. Lang, J. Appl. Phys. **45**, 3014 (1974).
[2] P. D. Kirchner, W. J. Schaff, G. N. Maracas, and L. F. Eastman, J. Appl. Phys. **52**, 6462 (1981).
[3] G. M. Martin, A. Mitonneau, and A. Mircea, Electron. Lett. **13**, 191 (1977).
[4] G. Vincent, A. Chantre, and D. Bois, J. Appl. Phys. **50**, 5484 (1979).
[5] S. Makram-Ebeid, Appl. Phys. Lett. **37**, 464 (1980).
[6] S. Makram-Ebeid, in *Defects in Semiconductors*, edited by J. Narayan and T. Y. Tan (North-Holland, New York, 1981), p. 495.
[7] G. P. Li and K. L. Wang, Solid-State Electron. **26**, 825 (1983).
[8] G. P. Li and K. L. Wang, J. Appl. Phys. **57**, 1016 (1985).
[9] C. W. Wang, C. H. Wu, J. L. Boone, and C. L. Balestra, J. Electron. Mater. **22**, 165 (1993).
[10] H. Kukimoto, C. H. Heney, and F. R. Merritt, Phys. Rev. B **7**, 2486 (1973).
[11] J. Criado, A. Gomez, E. Calleja, and E. Munoz, Appl. Phys. Lett. **52**, 660 (1988).
[12] M. Tachikawa, M. Mizuta, and H. Kukimoto, Jpn. J. Appl. Phys. **23**, 1594 (1984).
[13] B. Balland, R. Blondeau, B. de Cremoux, and P. Hirtz, Thin Solid Films **65**, 275 (1980).
[14] B. Balland, J. L. Pavot, B. de Cremoux, and P. Hirtz, Phys. Status Solidi A **68**, 661 (1981).
[15] P. Omling, L. Samuelson, and H. G. Grimmeiss, J. Appl. Phys. **54**, 5117 (1983).
[16] J. Yoshino, M. Tachikawa, N. Matsuda, M. Mizuta, and H. Kukimoto, Jpn. J. Appl. Phys. **23**, L29 (1984).
[17] P. M. Mooney, J. Appl. Phys. **67**, R1 (1990).
[18] O. Kumagai, H. Kawai, Y. Moriand, and K. Kaneko, Appl. Phys. Lett. **45**, 1322 (1984).
[19] A. F. Tasch, Jr. and C. T. Sah, Phys. Rev. B **1**, 800 (1970).
[20] D. Pons and S. Makram-Ebeid, J. Phys. **40**, 1161 (1979).
[21] A. Mircea and A. Mitonneau, J. Phys. **40**, L31 (1979).
[22] P. A. Martin, B. G. Streetman, and K. Hess, J. Appl. Phys. **52**, 7409 (1980).
[23] J. R. Morante, J. Samitier, A. Cornet, and A. Herms, Appl. Phys. Lett. **45**, 1317 (1984).
[24] T. Pavelka and G. Ferenczi, Mater. Sci. Forum **38-41**, 803 (1989).
[25] J. Frenkel, Phys. Rev. **54**, 647 (1938).